Ocean Engineering 157 (2018) 87–95

Contents lists available at ScienceDirect

Ocean Engineering

journal homepage: www.elsevier.com/locate/oceaneng

Extrapolation of random wave field data via compressive sampling

Giovanni Malara [a,*], Ioannis A. Kougioumtzoglou [b], Felice Arena [a]

[a] Natural Ocean Engineering Laboratory (NOEL), "Mediterranea" University of Reggio Calabria, Loc. Feo di Vito, 89122, Reggio Calabria, Italy
[b] Department of Civil Engineering & Engineering Mechanics, Columbia University, New York, NY, 10027, USA

ARTICLE INFO

Keywords:
Compressive sampling
Sparse representation
Adaptive basis
Random wave field
Directional spectrum

ABSTRACT

Estimating the space-time characteristics of a sea state is of crucial importance to a number of engineering applications, such as the ones involving three-dimensional waves interacting with marine structures. In this context, developing a technique that allows extrapolating information about the wave field utilizing only a relatively small number of records is highly impactful, as it allows minimizing the use of expensive and sophisticated measurement techniques. In this paper, a Compressive Sampling (CS) based technique is developed for extrapolating free surface displacement data. The technique relies on a directional spectrum compatible sparse representation in conjunction with formulating and solving an L_1-norm optimization problem. Further, the accuracy of the developed technique is significantly enhanced via the use of an adaptive basis re-weighting procedure. Pertinent numerical examples demonstrate that the technique is capable of reconstructing the time history of a free surface displacement record successfully, while capturing the main features of the target frequency spectrum and of the cross-correlation function satisfactorily.

1. Introduction

Determining the spatial characteristics of a sea state is pivotal for ensuring that marine structures operate safely when subjected to rare extreme events. For instance, commonly utilized large body structures, such as breakwaters (both fixed and floating), are excited by wave fields exhibiting a well-defined spatial configuration in case of extreme events (Isaacson and Nwogu, 1987; Boccotti, 2014) that must be accounted for to prevent structural failures (Oumeraci, 1994). Another relevant example pertains to the emerging field of wave energy converters, where single point (buoy-like) energy harvesters are aimed to be installed in arrays with a specified spatial distribution. In this context, a given array is typically regarded as one system providing the grid network with electrical power. Therefore, determining the response of all harvesters simultaneously is of significant importance to optimizing the performance of both the energy harvesters and the electrical grid (Folley and Whittaker, 2009). A final example relates to the field of sea wave statistics. Recent research work (Fedele et al., 2009, 2011; Naess and Batsevych, 2010; Fedele, 2012; Romolo and Arena, 2015; Romolo et al., 2016) demonstrated that conventional time-domain analyses underestimate real sea wave statistics in space-time domain, and thus, introduce unsafe input data in the design process. In this regard, knowledge of spatial data is clearly indispensable for estimating the appropriate design wave height to be adopted in the design of a marine structure.

A number of instruments/methods have been developed for quantifying sea state spatial characteristics, such as wave gauges, ultrasonic instruments, wave buoys, synthetic aperture radar (Schulz-Stellenfleth and Lehner, 2004; Li et al., 2010), satellites (Chelton et al., 2001) and variational stereo cameras (Gallego et al., 2011; Fedele et al., 2013). Wave gauges and ultrasonic instruments can be used for retrieving information about the frequency spectrum or, in case of multiple sensors, about the directional spectrum of the free surface displacement. Similar information is provided by individual wave buoys via acceleration data post-processing (Tucker, 1989). These data are utilized for acquiring only local information (free surface data at a certain point in the time domain). Thus, they cannot be used for obtaining space-time information, unless affording the high cost associated with the installation of a quite large number of instruments over a certain area. Radars and satellites allow covering quite large areas, but they are unavoidably affected by limited resolution when it comes to relatively small spatial scales. To overcome the above limitations, stereo wave imaging has been proposed by the implementation of variational stereo cameras (Benetazzo et al., 2015). These techniques involve the use of two or more cameras recording free surface images over a certain area, which are post-processed via 3-D reconstruction algorithms for recovering measurements of the free surface displacement. In this context, the main

* Corresponding author.
E-mail addresses: giovanni.malara@unirc.it (G. Malara), ikougioum@columbia.edu (I.A. Kougioumtzoglou), arena@unirc.it (F. Arena).

https://doi.org/10.1016/j.oceaneng.2018.03.044
Received 29 November 2016; Received in revised form 9 March 2018; Accepted 13 March 2018

drawback of the technique relates to the significant processing power required. This has an impact on the quality of the reconstruction algorithms that are designed considering a trade-off between speed and accuracy. Further, an additional drawback relates to the occasional inability to record some areas. For instance, the occurrence of a large wave crest may impede a given camera to have visual contact with a part of the wave field, and thus, the stereo technique cannot reconstruct the associated portion of the wave field. Therefore, the record shows small "holes" in the measured wave field (Gallego et al., 2011).

This paper addresses the problem of extrapolating the time history of the free surface displacement at a certain location $(\tilde{x}_j,\tilde{y}_j)$ given recorded time histories at various other different known locations (x_i, y_i). The solution to this problem can be regarded as a tool for overtaking some of the limitations associated with the aforementioned methodologies. For example, given the free surface data recorded by few ultrasonic probes placed at relatively distant locations, we may determine free surface data at other locations without the need of several (expensive) sensors. Another example relates to the variational stereo technique: given a successfully recovered time history, we may extrapolate information pertaining to the "holes" directly from the already available data at no additional cost in terms of camera requirements.

The technique developed in the paper is based on Compressive Sampling (CS) ideas in conjunction with sparse representations. CS was first proposed in the field of seismology by Claerbout and Muir (1973), and was recently revitalized due to the results of Candes et al. (2006a), Candes and Tao (2006) and Donoho (2006) (see also Candes and Wakin (2008) Candes and Wakin (2008)), which contributed extensively to establishing a rigorous mathematical foundation for CS. Their results fostered CS applications to quite diverse disciplines (Qaisar et al., 2013), such as radar imaging (Baraniuk and Steeghs, 2007), face recognition (Qiao et al., 2010) and magnetic resonance image reconstruction (Trzasko and Manduca, 2009). Civil engineering applications have been proposed, as well. For instance, the structural health monitoring community has exploited CS to reduce the number of data required for monitoring and assessing the damage of civil infrastructures (Huang et al., 2014; Di Ianni et al., 2015; Tau Siesakul et al., 2015; Wang and Hao, 2015; Yang and Nagarajaiah, 2015; Zou et al., 2015; Klis and Chatzi, 2017). Further, Comerford et al. (2014, 2016) and Zhang et al. (2017a; 2017b) demonstrated that CS is effective also for reconstructing signals describing random environmental processes such as winds, earthquakes and sea waves, which are characterized by a relatively small number of dominant frequencies. Specifically, they developed a technique for determining the power spectral density function of a signal (either stationary or non-stationary) subject to missing data in the time domain, and showed that power spectra can be successfully estimated even in cases of highly limited data (even up to 80% missing data for some cases).

Although CS has already revolutionized the signal processing field, the ocean engineering community has neglected so far the capabilities of CS. In this context, the first applications were proposed by Bayındır (2015, 2016a, b) that utilized CS for conducting numerical simulations of nonlinear gravity waves and for the early identification of crossing rough seas, while Laface et al. (2017) proposed the technique for reconstructing free surface data in time domain.

In the following sections, a CS technique is developed for reconstructing a wave field based on a given set of recorded data. The technique involves a relatively sparse representation compatible with a certain directional spectrum in conjunction with appropriate L_1-norm minimization algorithms. It is demonstrated that the main features of frequency spectra and spatial cross-correlations are preserved during the extrapolation. It is noted that concepts and ideas developed in Comerford et al. (2016) are extended herein to account for the significantly more sophisticated case of directional spectrum, whereas it is demonstrated that an adaptation of the iterative procedure enhancement proposed by Comerford et al. (2014, 2017) is particularly beneficial to the herein considered numerical examples.

2. Overview on stochastic process representation of a sea state

This section reviews in a concise manner a typical stochastic process representation used in the context of linear water wave mechanics for describing the free surface displacement in an undisturbed wave field. Next, it introduces the main statistical quantities involved in the description of a random wave field.

A stationary homogeneous Gaussian random wave field is represented by the equation (Ochi, 2005)

$$\eta(x,y,t)=\sum_{i=1}^{N} a_i \cos(k_i y\cos\theta_i + k_i x\sin\theta_i - \omega_i t + \varepsilon_i), \tag{1}$$

where $\eta(x,y,t)$ is the free surface displacement calculated at a certain location (x,y) at a given time instant t, a_i are wave amplitudes, ω_i are frequencies such that $\omega_i \neq \omega_j$ if $i \neq j$, θ_i are wave directions, k_i are wave numbers and ε_i are random phase angles uniformly distributed over the interval $0 \leq \varepsilon_i\ 2\pi$. The wave numbers are directly related to the frequencies ω_i. Specifically, in deep waters, they are calculated as (Mei et al., 2005)

$$k_i=\frac{\omega_i^2}{g}, \tag{2}$$

g being the acceleration due to gravity.

Eq. (1) involves the superposition of a large number N of regular waves each having a certain frequency and direction. However, their amplitudes are related to ω_i and θ_i via the directional spectrum $S(\omega,\theta)$ according to the relation

$$S(\omega,\theta)\delta\omega\delta\theta=\sum_i \frac{1}{2}a_i^2, \text{for } \omega<\omega_i<\omega+\delta\omega \text{ and } \theta<\theta_i<\theta+\delta\theta \tag{3}$$

In this regard, note that the frequency spectrum $E(\omega)$ of the process is associated with the directional spectrum (3) by the equation

$$E(\omega)=\int_{-\pi}^{\pi} S(\omega,\theta)d\theta. \tag{4}$$

The statistical characteristics of the free surface displacement are directly estimated from the directional spectrum (Ochi, 2005; Boccotti, 2014). Specifically, the significant wave height H_s is given by

$$H_s=4\sqrt{\int_0^{\infty}\int_{-\pi}^{\pi} S(\omega,\theta)d\theta d\omega}, \tag{5}$$

where it is recognized that the quantity under the square root is the variance of the free surface displacement process; and the spatial cross-correlation is

$$C_{XY}(\tau)=E[\eta(x,y,t)\eta(x+X,y+Y,t+\tau)], \tag{6}$$

$E[\cdot]$ being the mathematical expectation operator; X and Y being space lags; and τ being a time lag. In this context, it is seen that $C_{00}(\tau)$ is the auto-correlation function and $C_{00}(0)$ is the variance of the free surface displacement process.

The cross-correlation (6) is readily calculated from the directional spectrum via the equation

$$C_{XY}(\tau)=\int_0^{\infty}\int_{-\pi}^{\pi} S(\omega,\theta)\cos(kY\cos\theta+kX\sin\theta-\omega\tau)d\theta d\omega. \tag{7}$$

3. Compressive sampling

The celebrated Shannon's theorem states that the sampling rate of a signal must be at least twice the maximum frequency present in the signal (Shannon, 1949). CS allows recovering signals even in case of "undersampling". That is, even if the sampling rate is smaller than the Nyquist rate. In this section, the fundamental CS assumptions and conditions (sparsity, incoherence and restricted isometry property) are reviewed for completeness. Next, the optimization problem involved in the

extrapolation of free surface data is formulated in conjunction with an adaptive iterative procedure for enhancing the accuracy of the extrapolated signal.

3.1. Sparsity, incoherence and restricted isometry property

Many signals associated with natural phenomena (such as sea wave displacements) can be represented, via a convenient basis, with much fewer coefficients than the ones required by the Shannon-Nyquist rate. In this regard, consider a free surface displacement time history expanded as

$$\eta(t) = \sum_{i=1}^{n} A_i(t) z_i, \tag{8}$$

where A_i are the components of an orthonormal basis and z_i are the coefficient sequences obtained by projecting η in the A_i-space. The free surface displacement has a sparse representation if several of the z_i coefficients have adequately small values, and thus, can be disregarded for its reconstruction. Once the coefficients are identified via appropriate optimization algorithms, sparsity allows pursuing efficient data compression and statistical estimation (Comerford et al., 2016).

The choice of the basis is guided by the property of incoherence. Specifically, CS is pursued by considering that the sampling domain and the (sparse) transform domain have a high degree of incoherence. For instance, regarding the Fourier basis, spikes in the frequency domain correspond to sinusoids in the time domain, and vice versa. This pair is maximally incoherent as a single coefficient characterizing the signal in the transform domain corresponds to a harmonic signal spanning the entire length of the sampling domain.

Next, the robustness of CS is guaranteed by the Restricted Isometry Property (RIP) (Candes and Tao, 2005): the sampling matrix **A** satisfies RIP if there exists a constant δ_K such that

$$(1-\delta_K)\|\mathbf{z}\|_{l2}^2 \le \|\mathbf{A}\mathbf{z}\|_{l2}^2 \le (1+\delta_K)\|\mathbf{z}\|_{l2}^2, \tag{9}$$

for every vector $\mathbf{z} = [z_1, z_2, \ldots, z_n]$ with at least K non-zero values.

This property ensures that **z** cannot be in the null space of **A**, or, equivalently, that any matrix composed of K randomly selected columns of **A** should have full rank and be nearly orthonormal. To demonstrate that RIP holds for a given matrix **A** is NP-hard (Candes et al., 2006b), however for some matrices, such as Gaussian random matrices (Fornasier and Rauhut, 2011), RIP holds with a high probability.

3.2. Signal reconstruction by L_1-norm minimization

Consider N free surface displacement time histories (each composed by n samples) available at certain locations (x_i,y_i). Next, the objective is to extrapolate and determine time histories at arbitrary M distinct points $(\tilde{x}_j\tilde{y}_j)$. For this purpose, define $\boldsymbol{\eta}$ the $(nN \times 1)$ column vector containing the known samples of the free surface displacement and **A** the $(nN \times n(N+M))$ sampling matrix. Then, the measurement vector **z** considered sparse is determined by solving the problem

$$\boldsymbol{\eta} = \mathbf{A}\mathbf{z}. \tag{10}$$

Eq. (10) constitutes an underdetermined problem with infinite solutions. Therefore, an additional constraint is imposed with the objective of determining a unique solution that is as sparse as possible.

It is known that the sparsest solution occurs when the L_0-norm of **z** is minimized. However, this optimization problem is non-convex with no known exact solution (Candes et al., 2006a). Instead, a known solution is available by minimizing the L_2-norm of **z**. In this context it can be readily shown that

$$\min\|\mathbf{z}\|_{l2} = \mathbf{A}^T(\mathbf{A}\mathbf{A}^T)^{-1}\boldsymbol{\eta}. \tag{11}$$

This solution minimizes **z** in a mean square sense, but, in general, does not lead to a sparse solution.

A convenient alternative to these constraints is given by the minimization of the L_1-norm. Indeed, L_1-norm still promotes sparsity and, in addition, gives rise to a convex optimization problem that can be solved, for instance, by a gradient based optimization method (Stanković et al., 2012). In this context, the optimization problem is recast in the linear programming form

$$\min\|\mathbf{z}\|_{l1} \cdot \text{subject to} \cdot \boldsymbol{\eta} = \mathbf{A}\mathbf{Z} \tag{12}$$

Considering the fact that **z** is usually only approximately sparse and that some noise is always included in the computed values, Eq. (12) takes the form

$$\min\|\mathbf{z}\|_{l1} \cdot \text{subject to} \cdot \|\boldsymbol{A}\boldsymbol{Z} - \boldsymbol{\eta}\|_{l2} \le e \tag{13}$$

where e denotes a tolerance value. This modification has the effect of applying intervals to the solution, further promoting sparsity.

3.3. Accuracy enhancement via an adaptive iterative procedure

As demonstrated in Comerford et al. (2014), eq. (12) (or eq. (13)) is rather straightforward to apply, however, this kind of treatment comes with certain limitations. One potential drawback relates to the significant computational effort required in case of large amounts of recorded data. The second issue relates to the fact that the reconstructed free surface spectrum may occasionally contain spurious large peaks at unanticipated frequency values. This situation occurs specifically when the number of available records is small and there is a significant number of unknown data.

To address the above issues, an enhancement of the technique is proposed in the ensuing analysis via adapting and extending the iterative procedure proposed by Comerford et al. (2014) to account for the extrapolation problem at hand. In particular, the measurement vector **z** is determined via the optimization problem

$$\min\|\mathbf{z}\|_{l1} \cdot \text{subject to} \cdot \boldsymbol{\eta} = \boldsymbol{A}\boldsymbol{W}\boldsymbol{z} \tag{14}$$

or, via the counterpart of eq. (13), where **W** is a reweighting matrix; see also Comerford et al. (2014).

The rationale of the method relates to the fact that the (diagonal) matrix **W** can be used for appropriately weighting the columns of the sampling matrix **A**. For this purpose, the elements of the matrix **W** are selected as the magnitudes of the components of **z**. This choice promotes sparsity as it allows "reducing" the contribution of the small components of the measurement vector, however, it has the drawback of requiring a preliminary estimate of **z**. In this regard, the L_2-norm solution is utilized herein as the associated explicit formula (11) requires a limited computational cost, while capturing the key components of the signal adequately. Next, the measurement vector **z** is determined by solving problem (14). The procedure is beneficial particularly when an ensemble of realizations is available (Comerford et al., 2014). However, field measurements involve unique realizations, which cannot be repeated. In this context, the method can be implemented by partitioning the records in small subsets. Thus, considering each subset as an independent realization.

The procedure is implemented as follows: at the first iteration the reweighting matrix is assumed equal to the identity matrix. Then, for each available realization, the approximate values of **z** are calculated by the equation

$$\mathbf{z} = (\mathbf{A}\mathbf{W})^T\left((\mathbf{A}\mathbf{W})(\mathbf{A}\mathbf{W})^T\right)^{-1}\boldsymbol{\eta}. \tag{15}$$

The magnitude of these values are used for estimating a second matrix $\mathbf{W_2}$ having null values when computed for the first realization, as

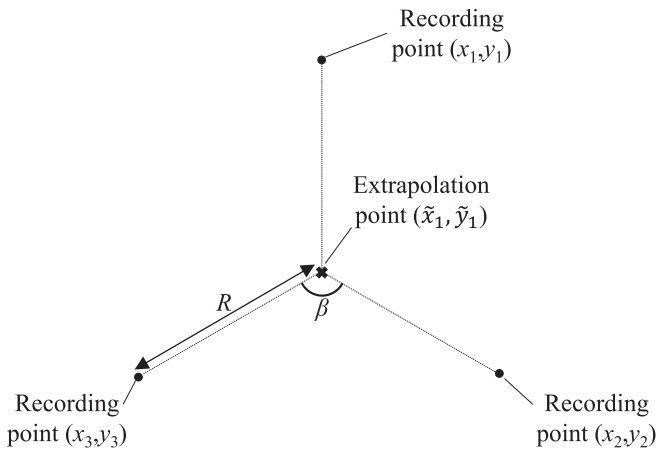

Fig. 1. Space distribution of the recording points and of the extrapolation point. Recording points are located at a constant distance R from the extrapolation point and uniformly distributed around the extrapolation point.

$$\mathbf{W}_2 = \mathbf{W}_2 + diag\left(\left[w_1, w_1, w_2, w_2, \ldots, w_{nN/2}, w_{nN/2}\right]\right), \tag{16}$$

where

$$w_i = \|z_{2i-1}, z_{2i}\|. \tag{17}$$

Once all the realizations have been processed, the reweighting matrix is calculated as

$$\mathbf{W} = \mathbf{W}_2, \tag{18}$$

and the procedure is iterated until converging to a certain matrix.

As a final step, the sparse measurement vector $\mathbf{z}$ is determined by eq. (14).

4. Numerical application

This section provides a numerical example where 3 recorded records of the free surface displacement are used for extrapolating information pertaining to a fourth point located at the centre of their spatial configuration (Fig. 1). The distance between the given points and the extrapolation point is R, while the points are uniformly distributed around the extrapolation one. In this regard, note that the choice of this particular configuration is absolutely arbitrary and is used only for simplifying the discussion and accommodating further analyses on the limits of the technique. Thus, other configurations with, for instance, more records at various distances from the extrapolation point (or points) can be adopted.

The realizations of the free surface displacement in deep water are obtained by numerical simulations relying on the representation (1) according to the method of Boccotti et al. (2011). Each time history is composed by $n = 120$ samples for a total duration of 60 s. The generated sea state is compatible with the directional spectrum

$$S(\omega,\theta) = E(\omega)D(\theta), \tag{19}$$

where $E(\omega)$ and $D(\theta)$ are a frequency spectrum and a directional spreading function, respectively. In this regard, the JONSWAP frequency spectrum (Hasselmann et al., 1973) is utilized in conjunction with a cosine power directional spreading function (Mitsuyasu et al., 1975). Specifically,

$$E(\omega) = \alpha g^2 \omega^{-5} \exp\left[-\frac{5}{4}\left(\frac{\omega}{\omega_p}\right)^{-4}\right] \exp\left\{\ln(\gamma)\exp\left[-\frac{(\omega-\omega_p)^2}{2\sigma^2\omega_p^2}\right]\right\}, \tag{20}$$

and

$$D(\theta) = \cos^{2s}\left[\frac{1}{2}(\theta-\theta_p)\right] \cdot \left[\int_0^{2\pi} \cos^{2s}\frac{1}{2}\theta\right]^{-1}. \tag{21}$$

The constants in eqs. (20) and (21) are: $\gamma = 3.3$;

$$\sigma = \begin{cases} 0.07 \text{ if } \omega < \omega_p \\ 0.09 \text{ if } \omega > \omega_p \end{cases};$$

$s = 20$; $\omega_p = 1{,}47$ rad/s; $\theta_p = 0°$; and $\alpha = 0.01$. The significant wave height of the generated sea states is $H_s = 1$ m.

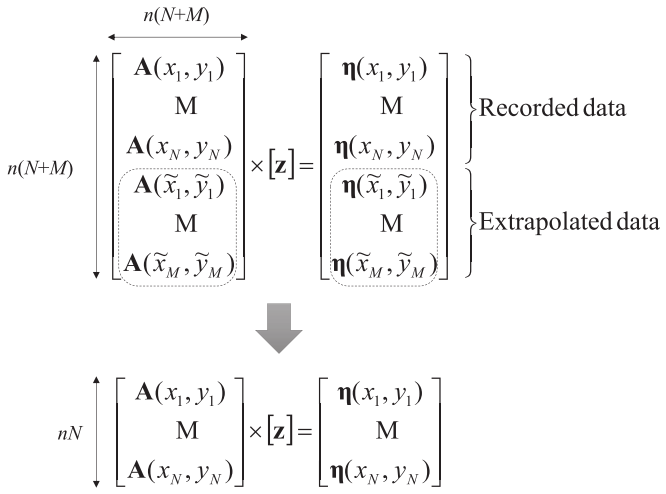

Fig. 2. Sampling matrix construction.

4.1. Sampling matrix construction

The full sampling matrix is constructed according to the representation adopted in eq. (1). Specifically, each individual time history of the free surface displacement at a given spatial point is associated with a matrix $\mathbf{A}(x_i,y_i)$ such that

$$\mathbf{A}(x_i,y_i) = \begin{bmatrix} \cos(\Xi_{1,i})\cos(\omega_1 t_1) & \sin(\Xi_{1,i})\sin(\omega_1 t_1) & \cdots & \cos\left(\Xi_{n(N+M)/2,i}\right)\cos\left(\omega_{n(N+M)/2} t_1\right) & \sin\left(\Xi_{n(N+M)/2,i}\right)\sin\left(\omega_{n(N+M)/2} t_1\right) \\ \vdots & \vdots & \vdots & \vdots & \vdots \\ \cos(\Xi_{1,i})\cos(\omega_1 t_n) & \sin(\Xi_{1,i})\sin(\omega_1 t_n) & \cdots & \cos\left(\Xi_{n(N+M)/2,i}\right)\cos\left(\omega_{n(N+M)/2} t_n\right) & \sin\left(\Xi_{n(N+M)/2,i}\right)\sin\left(\omega_{n(N+M)/2} t_n\right) \end{bmatrix}, \tag{22}$$

where

$$\Xi_{j,i} = k_j y_i \cos\theta_j + k_j x_i \sin\theta_j. \tag{23}$$

In this regard, note that the selection of the angles θ_j associated with the frequencies ω_j is conducted by the method described by Boccotti et al. (2011). Specifically, the directional domain is divided into n small intervals such that

$$\int_{\bar{\theta}_i}^{\bar{\theta}_{i+1}} D(\theta)d\theta = \frac{1}{n}. \tag{24}$$

From the directional domain, n wave angles are calculated by the

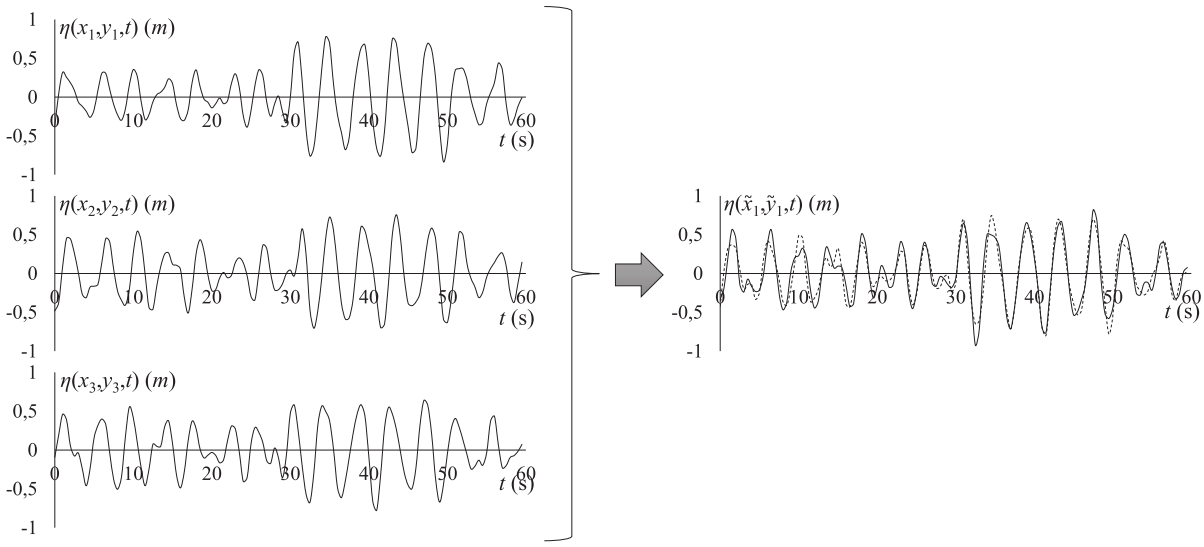

Fig. 3. Realizations of recorded (left panels) and of extrapolated (right panel) time histories of the free surface displacement. The right panel compares the free surface displacement computed by CS (continuous line) with the target free surface displacement (dotted line).

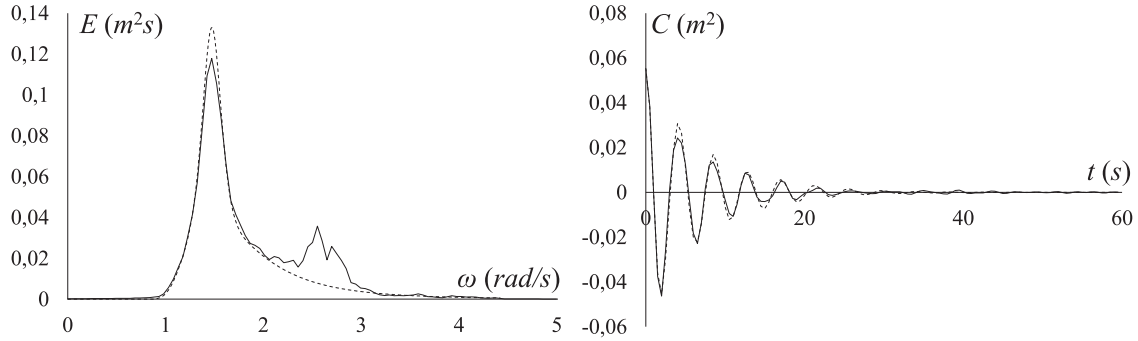

Fig. 4. Left panel: power spectral density function of the extrapolated signal vis-à-vis target power spectral density function. Right panel: cross-correlation between the extrapolated signal and the given signal $\eta(x_1,y_1,t)$. Continuous lines: computed values; dotted lines: target values. Extrapolation point – recording points distance $R = 0.1\ L_p$.

equation

$$\theta_i = \tilde{\theta}_i + (\tilde{\theta}_{i+1} - \tilde{\theta}_i)\tilde{\varepsilon}_i, \tag{25}$$

where $\tilde{\varepsilon}_i$ are random variables uniformly distributed over the interval (0,1). Then, each frequency ω_j is associated randomly with a certain direction θ_i.

Next, the full sampling matrix is constructed by assembling individual matrices associated with each record as shown in Fig. 2. Further, in the same figure it is shown that the vector on the right hand side is composed by vectors encapsulating the given values of the free surface displacement as

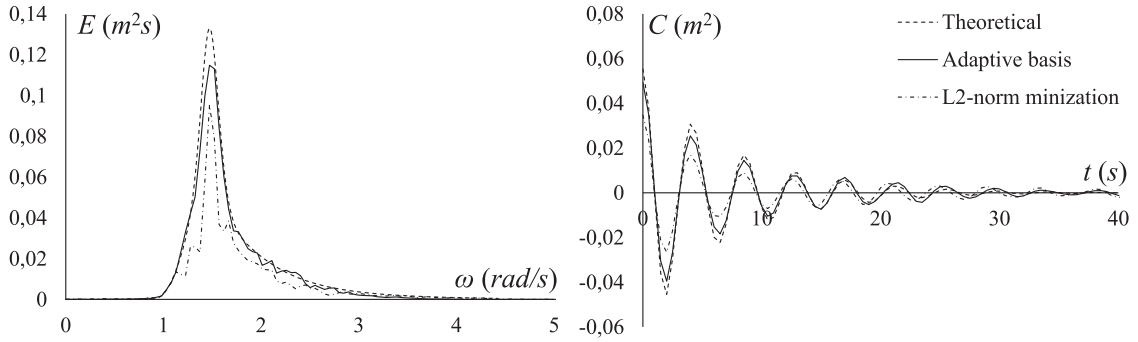

Fig. 5. Left panel: power spectral density function of the extrapolated signal vis-à-vis target power spectral density function. Right panel: cross-correlation between the extrapolated signal and the given signal $\eta(x_1,y_1,t)$. Extrapolation point – recording points distance $R = 0.1\ L_p$. Computations were pursued via adaptive basis and L_2-norm minimization.

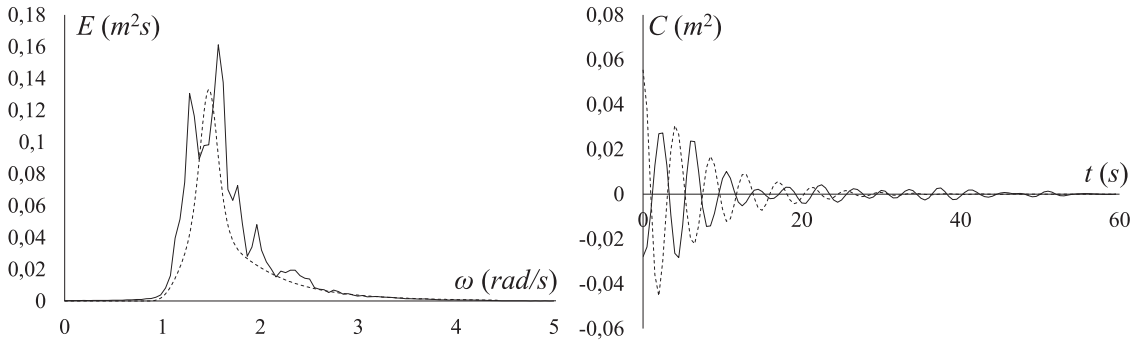

Fig. 6. Left panel: power spectral density function of the extrapolated signal vis-à-vis target power spectral density function. Right panel: cross-correlation between the extrapolated signal and the given signal $\eta(x_1,y_1,t)$. Continuous lines: computed values; dotted lines: target values. Extrapolation point – recording points distance $R = 0.5\ L_p$.

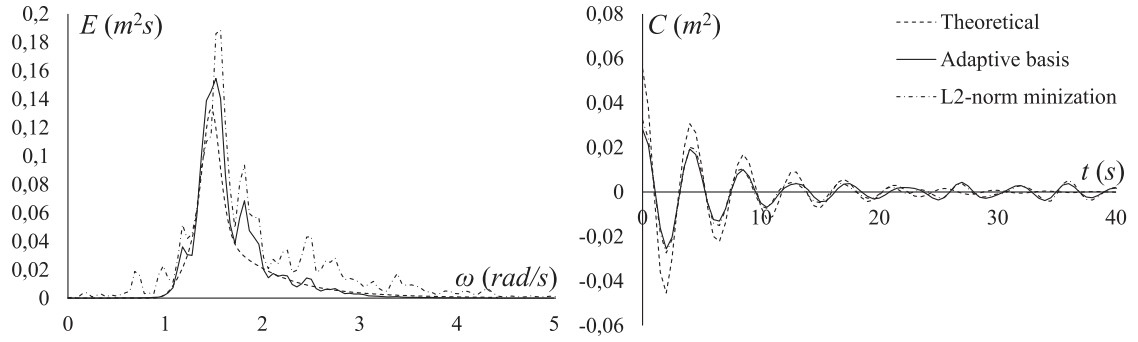

Fig. 7. Left panel: power spectral density function of the extrapolated signal vis-à-vis target power spectral density function. Right panel: cross-correlation between the extrapolated signal and the given signal $\eta(x_1,y_1,t)$. Extrapolation point – recording points distance $R = 0.5\ L_p$. Computations were pursued via adaptive basis and L_2-norm minimization.

$$\boldsymbol{\eta}(x_i, y_i) = \begin{bmatrix} \eta(x_i, y_i, t_1) \\ \vdots \\ \eta(x_i, y_i, t_n) \end{bmatrix}. \tag{26}$$

The underdetermined system utilized for estimating the sparse measurement vector **z** is obtained by removing from the full system the rows pertaining to the unknown free surface displacement data.

4.2. Extrapolation of the free surface displacement

An example of extrapolation is shown in Fig. 3. The figures show, on the left panel, the given time histories of the free surface displacement. Such time histories pertain to the same realization obtained via the representation (1) by utilizing the same set of random phase angles for all the records. The right panel compares the reconstructed free surface (continuous line) with the "true" free surface obtained within the numerical simulation (dotted line). In this regard, note that the reconstruction was pursued without resorting to the adaptive basis approach. This specific example has been pursued under the stipulation that the recording points are at a distance $R = 0.1\ L_p$, where L_p is the dominant wave length of the sea state. It is seen that the reconstruction accuracy of the free surface is quite satisfactory. Indeed, the periods of the individual waves are preserved during the reconstruction, while the crests and troughs are slightly either over- or under-estimated.

Fig. 4 shows comparisons regarding frequency spectra and cross-correlation functions. In this regard, note that the cross-correlation has been calculated by considering the time histories of points (x_1, y_1) and $(\tilde{x}_1, \tilde{y}_1)$, while the frequency spectrum of the free surface at the extrapolation point is calculated via the squared amplitudes of its Fourier components. Further, note that the results were obtained by averaging the results of 200 realizations. The frequency spectrum of the reconstructed signals captures the salient features of the original frequency spectrum (dotted line), but it also shows unexpected peaks occurring at the high frequency tail. This discrepancy was observed also by Comerford et al. (2014), and apparently, relates to the fact that a straightforward application of the L_1-norm minimization approach, as described in section 3.2, does not yield always the sparsest (or even a sparse enough) solution. This feature doesn't seem to affect the cross-correlation that, notably, retains a quite satisfactory accuracy degree during the reconstruction. Further, to enhance the accuracy, the adaptive basis is implemented. Fig. 5 shows that in this case a sparser solution is obtained, and thus, the unanticipated peaks are eliminated from the record and the frequency spectrum is reasonably well estimated over the entire frequency domain. A slight underestimation of the peak frequency value is noticed, however, the location of the peak is satisfactorily captured. Furthermore, the cross-correlation agrees well with the target cross-correlation. In addition, the figure shows a comparison with the results pertaining to the application of a L_2-norm minimization. In this case, it is seen that the results are markedly less representative of the target values. Indeed, the target spectrum is systematically underestimated over the entire frequency domain, as are the maxima and minima of the cross-correlation.

A crucial issue in the implementation of CS for extrapolation purposes is the distance between the extrapolation point and the recording point. Figs. 6 and 7 show the results pertaining to the case where the distance $R = 0.5\ L_p$. In a similar manner as in the previous example, CS is utilized without (Fig. 6) and with (Fig. 7) the adaptive basis. It is seen that the quality of the reconstruction deteriorates if the recording points are far from the extrapolation point. However, the use of the adaptive basis allows preserving the main features of the cross-correlation that, otherwise, are completely lost. As in the previous example, the use of a L_2-norm minimization provides with a significantly worse extrapolation

result as compared to the proposed adaptive basis. Indeed, although the cross-correlations are quite similar to each other, it is seen that the L_2-norm overestimates the frequency spectrum over the whole frequency domain and introduces rather large unrealistic peaks at both low and high frequencies.

A more general overview on this last issue is given in Fig. 8, where the correlation coefficient $\rho(A,B)$ given by the equation

$$\rho(A,B) = \frac{\mathrm{cov}(A,B)}{\sigma_A \sigma_B}, \tag{27}$$

cov (A,B) being the covariance between A and B and σ_A and σ_B being the standard deviations of A and B, respectively, is used for measuring the similarity between the simulated free surface displacements and the reconstructed free surface displacements. It is seen that the similarity between the signals rapidly decays with the distance from the recording points. The graph is limited to the interval $R/L_{p0} = (0, 1)$, as numerical computations showed that larger values lead to uncorrelated free surface displacement data.

4.3. Extrapolation of nonlinear free surface data

There is a general consensus about the fact that realistic representations of the free surface displacement must account for nonlinear (second order in a Stokes' expansion) effects. Indeed, sea waves exhibit sharp crests and flat troughs producing deviations of the crest and trough distributions from the Rayleigh distribution, which are not captured via the linear water wave theory (Arena and Guedes Soares, 2009).

Herein, the CS approach is employed via the formulation described in the previous sections by utilizing nonlinear free surface displacement data. The rationale of this numerical example is evaluating to what extent this formulation is eligible for applications in real seas, where nonlinearity may play a significant role. In this context, the input data and the target free surface displacement at the point $(\tilde{x}_1 \tilde{y}_1)$ are simulated numerically via the method described by Romolo et al. (2014), which produces a free surface displacement compatible with a random second order Stokes' wave by superposing a linear wave to a second order contribution. For comparison purposes, the reconstruction is conducted also by utilizing exclusively the underlying linear free surface displacement. Finally, the correlation coefficient is calculated for both cases in order to check if introducing nonlinearities in the free surface may deteriorate the quality of the reconstruction. This numerical example considers three sea states with identical $H_S = 4$ m, and different peak spectral periods $T_p = 8{,}5$ s, 7 s, and 6 s. These three sea states have steepness coefficient $S_p = 0.035$, 0.052 and 0.071, respectively (Forristall, 2000). In all cases, the simulated time window is 120 s.

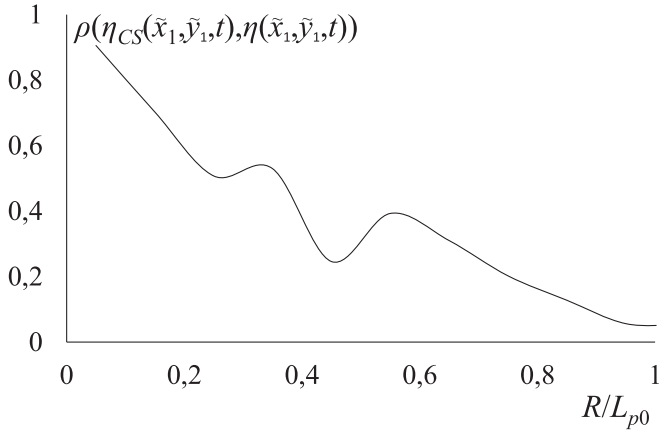

Fig. 8. Correlation coefficient between the simulated free surface $\eta(\tilde{x}_1,\tilde{y}_1,t)$ and the reconstructed free surface $\eta_{CS}(\tilde{x}_1,\tilde{y}_1,t)$ as a function of the distance between the extrapolation point and the recording points.

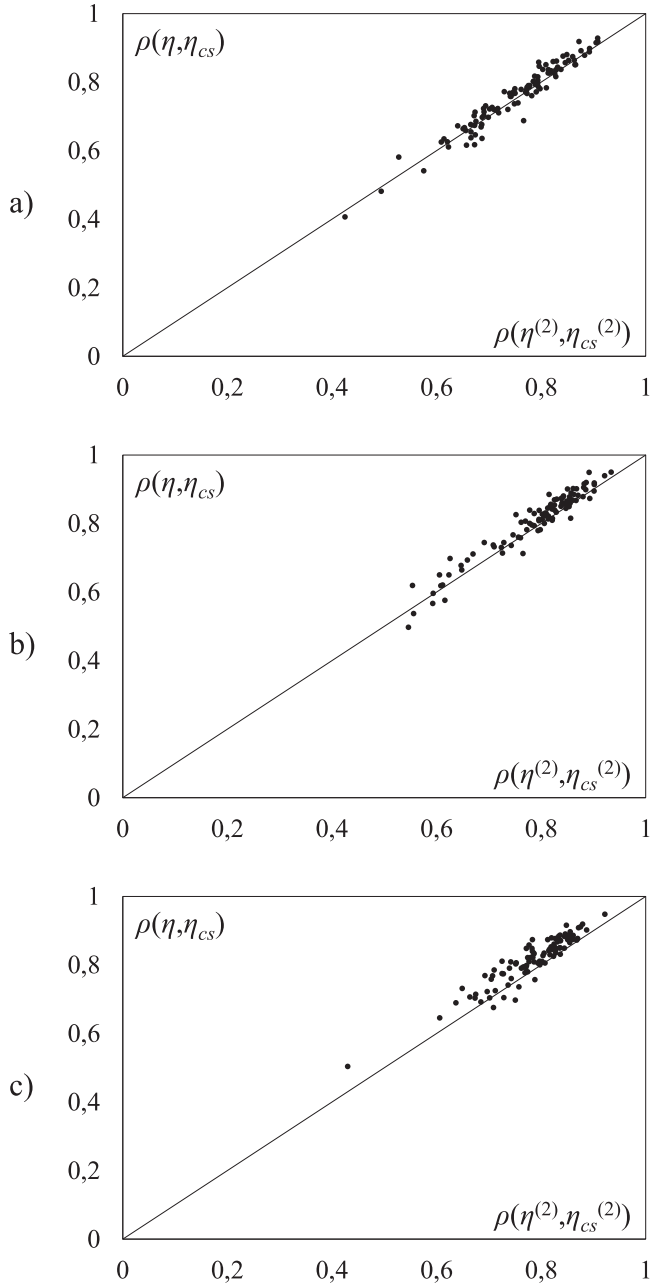

Fig. 9. Correlation coefficient by nonlinear free surface waves vis-à-vis correlation coefficient by linear surface waves for 100 realizations. Extrapolation point – recording points distance $R = 0.1\ L_p$. Panel a): sea state with steepness parameter 0.035; panel b): steepness parameter 0.052; panel c): steepness parameter 0.071.

Fig. 9 shows the correlation coefficients calculated by using the nonlinear waves vis-à-vis the correlation coefficient calculated by using the linear waves. The calculation is pursued by assuming $R = 0.1\ L_p$. Totally, 100 realizations of the free surface displacement have been synthesized in each case. The figure shows that the reconstruction via nonlinear free surface is affected by a small decrease of the correlation coefficient with respect to the linear case, with ±15% variation of the correlation coefficient with respect to the linear wave reconstruction. This evidence is observed also by considering the average value of the correlation coefficient. Indeed, Table 1 shows that the greatest discrepancy pertains to the steeper sea state, while no substantial difference is observed in case of low steepness.

Table 1
Correlation coefficient (27) calculated from linear and nonlinear simulated waves pertaining to sea states with various steepness parameters.

Sea state parameters			Correlation coefficients	
H_s [m]	T_p [s]	Steepness	Linear waves	Nonlinear waves
4	8.53	0.035	0.758	0.752
4	7	0.052	0.807	0.790
4	6	0.071	0.816	0.786

5. Concluding remarks

Compressive Sampling (CS) has revolutionized the signal processing field by allowing sampling signals without the constraint of the Nyquist rate. To date, the ocean engineering community has marginally considered CS as a potent tool for sea waves processing. In this paper, a CS based technique has been developed for extrapolating free surface displacement time histories. The technique relies on the identification of a sampling matrix ensuring: determination of a sparse measurement vector; incoherence between bases in the sampling and the transform domains; and validity of the restricted isometry property.

The paper has demonstrated that the CS based technique can successfully recover the time history of the free surface displacement given free surface data recorded at various other locations. It has been shown that the quality of the reconstruction is highly dependent on the distance between the extrapolation point and the recording point. Indeed, for relatively large distances the quality of the extrapolation deteriorates. In this regard, it was observed that reliable data are extrapolated at a distance of 0.1 L_p (L_p being the dominant wave length of the sea state), while the reconstruction is rather rough for distances of 0.5 L_p. Note that the utilization of an adaptive basis in the technique has drastically improved its accuracy, and has addressed the above limitation at a large extent. In fact, the enhanced technique has reconstructed the target frequency spectrum more accurately, while capturing at the same time the main features of the cross-correlation between free surface displacement data. The herein proposed L_1-norm technique has shown to exhibit superior accuracy to a standard L_2-norm minimization technique, which determined unrealistic peaks in the spectrum at both low and high frequencies.

In view of the implementation with real field data, the technique has been implemented also in conjunction with nonlinear free surface data. The numerical results have shown that the reconstruction is slightly less accurate with respect to the case of linear waves. This observation appears more evident in quite steep seas, where nonlinear effects are important. In this regard, future studies focusing on situations where nonlinear effects are significant (for instance, waves in finite water depth, or in inhomogeneous wave fields) may be pursued in conjunction with the use of real (measured) field data.

Acknowledgement

This paper was developed during the Marie Curie IRSES project “Large Multi- Purpose Platforms for Exploiting Renewable Energy in Open Seas (PLENOSE)” funded by the European Union (Grant Agreement Number: PIRSES-GA-2013-612581). G. Malara is grateful to ENEA (Agenzia nazionale per le nuove tecnologie, l'energia e lo sviluppo economico sostenibile) for funding his activity by the postdoctoral fellowship “Experimental and full scale analysis of wave energy devices”. I.A. Kougioumtzoglou gratefully acknowledges the support by the CMMI Division of the National Science Foundation, USA (Award number: 1724930). The authors gratefully acknowledge Dr. Alessandra Romolo for the fruitful technical discussion about nonlinear waves.

References

Arena, F., Guedes Soares, C., 2009. Nonlinear crest, trough, and wave height distributions in sea states with double-peaked spectra. J. Offshore Mech. Arct. Eng. 131 (4), 1–8.
Baraniuk, R., Steeghs, P., 2007. Compressive radar imaging. In: Proceedings of the IEEE National Radar Conference - Proceedings.
Bayındır, C., 2015. Compressive Spectral Method for the Simulation of the Water Waves arXiv:1512.06286v1 [physics.Comp-ph].
Bayındır, C., 2016a. Compressive spectral method for the simulation of the nonlinear gravity waves. Sci. Rep. 6, 22100.
Bayındır, C., 2016b. Early Detection of Rogue Waves Using Compressive Sensing arXiv: 1602.00816v1 [physics.Flu-dyn].
Benetazzo, A., Barbariol, F., Bergamasco, F., Torsello, A., Carniel, S., Sclavo, M., 2015. Observation of extreme sea waves in a space–time ensemble. J. Phys. Oceanogr. 45 (9), 2261–2275.
Boccotti, P., 2014. Wave Mechanics and Wave Loads on Marine Structures. Butterworth-Heinemann, Oxford.
Boccotti, P., Arena, F., Fiamma, V., Romolo, A., Barbaro, G., 2011. Estimation of mean spectral directions in random seas. Ocean. Eng. 38 (2–3), 509–518.
Candes, E.J., Romberg, J., Tao, T., 2006a. Robust uncertainty principles: exact signal reconstruction from highly incomplete frequency information. IEEE Trans. Inf. Theory 52 (2), 489–509.
Candes, E.J., Romberg, J.K., Tao, T., 2006b. Stable signal recovery from incomplete and inaccurate measurements. Commun. Pure Appl. Math. 59 (8), 1207–1223.
Candes, E.J., Tao, T., 2005. Decoding by linear programming. IEEE Trans. Inf. Theory 51 (12), 4203–4215.
Candes, E.J., Tao, T., 2006. Near-Optimal signal recovery from random projections: universal encoding strategies? IEEE Trans. Inf. Theory 52 (12), 5406–5425.
Candes, E.J., Wakin, M.B., 2008. An introduction to compressive sampling. IEEE Signal Process. Mag. 25 (2), 21–30.
Chelton, D.B., Ries, J.C., Haines, B.J., Fu, L.-L., Callahan, P.S., 2001. Chapter 1 satellite altimetry. In: Lee-Lueng, F., Anny, C. (Eds.), International Geophysics. Academic Press, pp. 1–2.
Claerbout, J.F., Muir, F., 1973. Robust modeling with erratic data. Geophysics 38 (5), 826–844.
Comerford, L., Jensen, H.A., Mayorga, F., Beer, M., Kougioumtzoglou, I.A., 2017. Compressive sensing with an adaptive wavelet basis for structural system response and reliability analysis under missing data. Comput. Struct. 182, 26–40.
Comerford, L., Kougioumtzoglou, I.A., Beer, M., 2016. Compressive sensing based stochastic process power spectrum estimation subject to missing data. Probabilistic Eng. Mech. 44, 66–76.
Comerford, L.A., Beer, M., Kougioumtzoglou, I.A., 2014. Compressive sensing based power spectrum estimation from incomplete records by utilizing an adaptive basis. In: Proceedings of the IEEE Symposium on Computational Intelligence for Engineering Solutions (CIES).
Di Ianni, T., De Marchi, L., Perelli, A., Marzani, A., 2015. Compressive sensing of full wave field data for structural health monitoring applications. IEEE Trans. Ultrasonics, Ferroelectr. Freq. Control 62 (7), 1373–1383.
Donoho, D.L., 2006. Compressed sensing. IEEE Trans. Inf. Theory 52 (4), 1289–1306.
Fedele, F., 2012. Space–time extremes in short-crested storm seas. J. Phys. Oceanogr. 42 (9), 1601–1615.
Fedele, F., Arena, F., Tayfun, M.A., 2011. Space-time extremes in sea storms. In: Proceedings of the ASME 2011 30th International Conference on Ocean, Offshore and Arctic Engineering - OMAE2011. Rotterdam, The Netherlands.
Fedele, F., Benetazzo, A., Gallego, G., Shih, P.-C., Yezzi, A., Barbariol, F., Ardhuin, F., 2013. Space–time measurements of oceanic sea states. Ocean. Model. 70, 103–115.
Fedele, F., Sampath, P., Gallego, G., Yezzi, A., Benetazzo, A., Tayfun, M.A., Forristall, G.Z., Cavaleri, L., Sclavo, M., Bastianini, M., 2009. Beyond waves & spectra: euler characteristics of oceanic sea states. In: Proceedings of the 28th International Conference on Ocean, Offshore and Arctic Engineering, OMAE2009, Honolulu, HI.
Folley, M., Whittaker, T.J.T., 2009. The effect of sub-optimal control and the spectral wave climate on the performance of wave energy converter arrays. Appl. Ocean Res. 31 (4), 260–266.
Fornasier, M., Rauhut, H., 2011. Compressive sensing. In: Scherzer, O. (Ed.), Handbook of Mathematical Methods in Imaging. Springer New York, New York, NY, pp. 187–228.
Forristall, G.Z., 2000. Wave crest distributions: observations and second-order theory. J. Phys. Oceanogr. 30 (8), 1931–1943.
Gallego, G., Yezzi, A., Fedele, F., Benetazzo, A., 2011. A variational stereo method for the three-dimensional reconstruction of ocean waves. IEEE Trans. Geoscience Remote Sens. 49 (11), 4445–4457.
Hasselmann, K., Barnett, T.P., Bouws, E., Carlson, H., Cartwright, D.E., Eake, K., Euring, J.A., Gicnapp, A., Hasselmann, D.E., Kruseman, P., Meerburg, A., Mullen, P., Olbers, D.J., Richren, K., Sell, W., Walden, H., 1973. Measurements of wind-wave growth and swell decay during the joint North Sea wave project (JONSWAP). Ergänzungsh. zur Dtsch. Hydrogr. Z. A8, 1–95.
Huang, Y., Beck, J.L., Wu, S., Li, H., 2014. Robust bayesian compressive sensing for signals in structural health monitoring. Computer-Aided Civ. Infrastructure Eng. 29 (3), 160–179.
Isaacson, M., Nwogu, O.U., 1987. Wave loads and motions of long structures in directional seas. J. Offshore Mech. Arct. Eng. 109 (2), 126–132.
Klis, R., Chatzi, E.N., 2017. Vibration monitoring via spectro-temporal compressive sensing for wireless sensor networks. Struct. Infrastructure Eng. 13 (1), 195–209.

Laface, V., Kougioumtzoglou, I.A., Malara, G., Arena, F., 2017. Efficient processing of water wave records via compressive sensing and joint time-frequency analysis via harmonic wavelets. Appl. Ocean Res. 69, 1–9.
Li, X., Lehner, S., Rosenthal, W., 2010. Investigation of ocean surface wave refraction using TerraSAR-x data. IEEE Trans. Geoscience Remote Sens. 48 (2), 830–840.
Mei, C.C., Stiassnie, M., Yue, D.K.P., 2005. Theory and Applications of Ocean Surface Waves: Linear Aspects ; Part 2, Nonlinear Aspects. World Scientific, Singapore.
Mitsuyasu, H., Tasai, F., Suhara, T., Mizuno, S., Ohkusu, M., Honda, T., Rikiishi, K., 1975. Observations of the directional spectrum of ocean WavesUsing a cloverleaf buoy. J. Phys. Oceanogr. 5 (4), 750–760.
Naess, A., Batsevych, O., 2010. Space-time extreme value statistics of a Gaussian random field. Probabilistic Eng. Mech. 25 (4), 372–379.
Ochi, M.K., 2005. Ocean Waves: the Stochastic Approach. Cambridge University Press, Cambridge, United Kingdom.
Oumeraci, H., 1994. Review and analysis of vertical breakwater failures — lessons learned. Coast. Eng. 22 (1), 3–29.
Qaisar, S., Bilal, R.M., Iqbal, W., Naureen, M., Lee, S., 2013. Compressive sensing: from theory to applications, a survey. J. Commun. Netw. 15 (5), 443–456.
Qiao, L., Chen, S., Tan, X., 2010. Sparsity preserving projections with applications to face recognition. Pattern Recognit. 43 (1), 331–341.
Romolo, A., Arena, F., 2015. On Adler space-time extremes during ocean storms. J. Geophys. Res. Oceans 120 (4), 3022–3042.
Romolo, A., Arena, F., Laface, V., 2014. A generalized approach to the mechanics of three-dimensional nonlinear ocean waves. Probabilistic Eng. Mech. 35, 96–107.
Romolo, A., Malara, G., Laface, V., Arena, F., 2016. Space–time long-term statistics of ocean storms. Probabilistic Eng. Mech. 44, 150–162.
Schulz-Stellenfleth, J., Lehner, S., 2004. Measurement of 2-D sea surface elevation fields using complex synthetic aperture radar data. IEEE Trans. Geoscience Remote Sens. 42 (6), 1149–1160.
Shannon, C., 1949. Comunication in the presence of noise. Proc. Inst. Radio Eng. 37 (1), 10–21.
Stanković, S., Orović, I., Sejdić, E., 2012. Compressive Sensing, Multimedia Signals and Systems. Springer US, Boston, MA, pp. 233–254.
Tau Siesakul, B., Gkoktsi, K., Giaralis, A., 2015. Compressive power spectrum sensing for vibration-based output-only system identification of structural systems in the presence of noise. In: Proceedings of the SPIE Sensing Technology + Applications, International Society for Optics and Photonics.
Trzasko, J., Manduca, A., 2009. Highly undersampled magnetic resonance image reconstruction via homotopic l0-minimization. IEEE Trans. Med. Imaging 28 (1), 106–121.
Tucker, M.J., 1989. Interpreting directional data from large pitch-roll-heave buoys. Ocean. Eng. 16 (2), 173–192.
Wang, Y., Hao, H., 2015. Damage identification scheme based on compressive sensing. J. Comput. Civ. Eng. 29 (2).
Yang, Y., Nagarajaiah, S., 2015. Output-only modal identification by compressed sensing: non-uniform low-rate random sampling. Mech. Syst. Signal Process. 56, 15–34.
Zhang, Y., Comerford, L., Kougioumtzoglou, I., Beer, M., 2017a. Lp-norm minimization for stochastic process power spectrum estimation subject to incomple data. Mech. Syst. Signal Process. 101, 361–376.
Zhang, Y., Comerford, L., Kougioumtzoglou Ioannis, A., Patelli, E., Beer, M., 2017b. Uncertainty quantification of power spectrum and spectral moments estimates subject to missing data. ASCE-ASME J. Risk Uncertain. Eng. Syst. Part A Civ. Eng. 3 (4), 04017020.
Zou, Z., Bao, Y., Li, H., Spencer, B.F., Ou, J., 2015. Embedding compressive sensing-based data loss recovery algorithm into wireless smart sensors for structural health monitoring. IEEE Sensors J. 15 (2), 797–808.